*sustainability*

MDPI

*Article*

# The Single-Channel Microseismic Mine Signal Denoising Method and Application Based on Frequency Domain Singular Value Decomposition (FSVD)

**Quanjie Zhu [1,*], Longkun Sui [2], Qingsong Li [3], Yage Li [4], Lei Gu [2] and Dacang Wang [2]**

[1] School of Emergency Technology and Management, North China Institute of Science and Technology, Langfang 065201, China
[2] School of Mine Safety, North China Institute of Science and Technology, Langfang 065201, China; slkyyds@163.com (L.S.)
[3] Guizhou Coal Mine Design & Research Institute, Guiyang 550025, China
[4] Science and Technology Innovation Department, China National Coal Group Corp, Beijing 100120, China; Jacob_868@foxmail.com
* Correspondence: zhqj2016@ncist.edu.cn

**Abstract:** The purpose of denoising microseismic mine signals (MMS) is to extract relevant signals from background interference, enabling their utilization in wave classification, identification, time analysis, location calculations, and detailed mining feature analysis, among other applications. To enhance the signal-to-noise ratio (*SNR*) of single-channel MMS, a frequency-domain denoising method based on the Fourier transform, inverse transform, and singular value decomposition was proposed, along with its processing workflow. The establishment of key parameters, such as time delay, $\tau$, reconstruction order, $k$, Hankel matrix length, $n$, and dimension, m, were introduced. The reconstruction order for SVD was determined by introducing the energy difference spectrum, E, and the denoised two-dimensional microseismic time series was obtained based on the SVD recovery principle. Through the analysis and processing of three types of typical microseismic waveforms in mining (blast, rock burst, and background noise) and with the evaluation of four indicators, *SNR*, *ESN*, *RMSE*, and *STI*, the results show that the *SNR* is improved by more than 10 dB after FSVD processing, indicating a strong noise suppression capability. This method is of significant importance for the rapid analysis and processing of microseismic signals in mining, as well as subsequently and accurately picking the initial arrival times and the exploration and analysis of microseismic signal characteristics in mines.

**Keywords:** microseismic signal; noise reduction; singular value decomposition; Fourier transform; arrival time picking

check for updates

**Citation:** Zhu, Q.; Sui, L.; Li, Q.; Li, Y.; Gu, L.; Wang, D. The Single-Channel Microseismic Mine Signal Denoising Method and Application Based on Frequency Domain Singular Value Decomposition (FSVD). *Sustainability* **2023**, *15*, 10588. https://doi.org/10.3390/su151310588

Academic Editors: Wei Yang, Xu Yu and Chunchen Wei

Received: 18 May 2023
Revised: 19 June 2023
Accepted: 23 June 2023
Published: 5 July 2023

**Copyright:** © 2023 by the authors. Licensee MDPI, Basel, Switzerland. This article is an open access article distributed under the terms and conditions of the Creative Commons Attribution (CC BY) license (https://creativecommons.org/licenses/by/4.0/).

## 1. Introduction

With the expansion of mining areas and the increase in mining depth, the number of microseismic mine events has gradually increased. Microseismic monitoring technology is widely used in mines due to its unique characteristics and advantages. Microseismic monitoring technology is a technology used to monitor weak vibration signals in underground rocks or surface structures. It is often used to monitor and evaluate the final fracturing effect in oil and gas, mining, and other fields [1,2]. However, the amount of microseismic monitoring data is huge, and there is complex background noise interference, which is inconvenient for later data processing and analysis [3,4]. Therefore, in microseismic monitoring technology, noise reduction and the filtering of microseismic mine signals are important prerequisites for rapid and accurate analysis.

The hydraulic fracturing area of the coal seam is at the level of 100 m, which belongs to small-scale microseismic monitoring. The sensors are adjacent to each other in the same coal

seam, so the difference between the coal seam and the medium propagation environment is relatively small [5,6]. It is difficult to reduce noise using conventional time-domain and frequency-domain analysis methods. Therefore, experts locally and abroad have proposed many denoising methods for non-stationary, nonlinear, and transient signals, such as bandpass filtering (BF), EMD filtering, wavelet packet threshold filtering (WPTF), FK-domain filtering, Butterworth filtering (BWF), and Chebyshev filtering [7]. In addition, in practical engineering, frequency domain analysis, virtual response function, and iterative optimization can better provide reasonable parameter selection for engineering structures so as to provide an important basis for safety monitoring [8–10].

Singular value decomposition (SVD) has shown remarkable effectiveness in the fields of mechanical engineering and geophysics since the 1980s [11,12]. At present, the SVD method has been successfully applied in characteristic signals extraction [13], noise suppression [14–16], wave field separation [17,18], signal identification [19], onset time picking [20–22], and seismic inversion [23]. The SVD method has been used for seismic data noise suppression and wave field separation based on the predominant properties in matrix data compression and the fine description of signal sequence characteristics [24]. However, while using singular value decomposition has certain advantages in noise suppression and feature extraction, it also has some limitations. If there are too many interference components, the denoising effect may be poor.

Based on the above reasons and on the premise of drawing lessons from previous studies, this paper proposes the construction method of the Hankel matrix for single-channel microseismic signals and proposes a method for single-channel microseismic mine signal denoising based on frequency domain SVD combined with the Fourier transform, inverse transform, and SVD. This method establishes the delay time, $\tau$, reconstruction order, $k$, Hankel matrix length, $n$, and dimension, $m$, and other key parameters are selected. The singular value energy difference spectrum, E, is introduced to determine the reconstruction order of SVD so as to obtain the two-dimensional microseismic time series after noise reduction. This method has practical significance in the extraction, feature extraction, and analysis of microseismic signals and has important practical value in promoting the sustainable development of the mining industry.

## 2. Background

### *2.1. Rock Burst Hazards*

With the gradual depletion of shallow coal resources, mining will gradually shift deeper. Taking rock bursts and coal and gas outburst accidents as examples, these disasters will start to occur frequently. Figure 1 shows a typical accident in a coal mine: (a) a rock burst accident in a coal mine and (b) a coal and gas outburst accident in a coal mine.



(**a**) (**b**)

**Figure 1.** Typical accidents involving coal or rock dynamic disasters in a mine. (**a**) Equipment damage in the roadway. (**b**) Large deformation of the roadway.

Hydraulic fracturing technology is an essential method for addressing gas protrusion and impact pressure issues in coal mines. It is a "green mining" technique that encompasses various characteristics, such as reducing rock strength, diluting gas, and mitigating dust

and temperature. The geometric diagram of hydraulic fracturing technology is shown in Figure 2. Hydraulic fracturing technology injects fracturing fluid into the well using a high-pressure water pump, creating one or multiple fractures. Proppant-laden fracturing fluid is then injected into the fractures to keep them open and prevent closure. After the pumping stops, a sufficiently long, wide, and high fracture is obtained. Hydraulic fracturing technology is widely used in mining fields, such as ground stress measurement, stress directional transfer and relief, weakening and damping of rock strength, coalbed methane extraction, enhancement of gas-bearing coal seam permeability, and sudden-onset abatement.

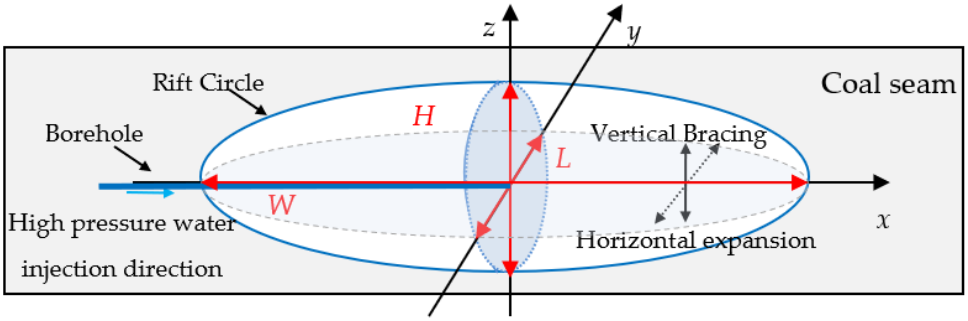



**Figure 2.** Schematic diagram of hydraulic fracturing geometry.

### *2.2. The Quantitative Evaluation Method of the Coal Seam Hydraulic Fracturing Effect Based on Microseismic Mine Signals*

The working-face, coal-body side of the 41,101 working-face return airway was selected as the test area for this project, with a length of about 150 m. The site fracture hole layout is shown in Figure 3. A total of 3 fracture holes with 8 m spacing, a 94 mm hole diameter, and different hole depths were arranged in this working face, with hole #1 at a depth of 38.9 m and holes #2 and #3 at a depth of 60 m with a 65 mm hole diameter. The length of the fracture test section was 55 m. From Figure 3, it can be seen that the large-diameter coal seam pressure relief boreholes were constructed before and after the test section, and only the large-diameter coal seam pressure relief boreholes were not constructed in the test section to ensure the comparison with the coal seam that had not been tested after the completion of fracturing. Regarding them, the diameter of the pressure relief borehole was 150 mm, the depth of the borehole was 25 m, and the spacing was 2 m. The hole was sealed with a special hole sealer 2 m in front and behind the fracturing section, and the length of the fracturing section was 1 m. The hole sealer had a compressive strength of 40 Mpa and an outer diameter of 55 mm; it could slide back and forth in the hole according to the design's fracturing requirements, thus realizing the fracturing of the entire coal seam into predetermined "small pieces". Outside the hole sealer, a seamless steel pipe was used to connect to the hole, and a quick connector was used to connect to the high-pressure hose. The change process of the microseismic signal obtained from the fracturing test is shown in Figure 4.

Based on the above research background, this study adopts advanced microseismic technology as a monitoring tool and extracts a "clean" microseismic signal by denoising the microseismic signal in the process of coal seam hydraulic fracturing so as to realize the microseismic quantitative analysis and evaluation of the effect of coal seam hydraulic fracturing. This study provides a basis for promoting the application of hydraulic fracturing technology in a coal mine field and has scientific significance for coal seam gas exploitation, impact pressure, and coal and gas outburst prevention.

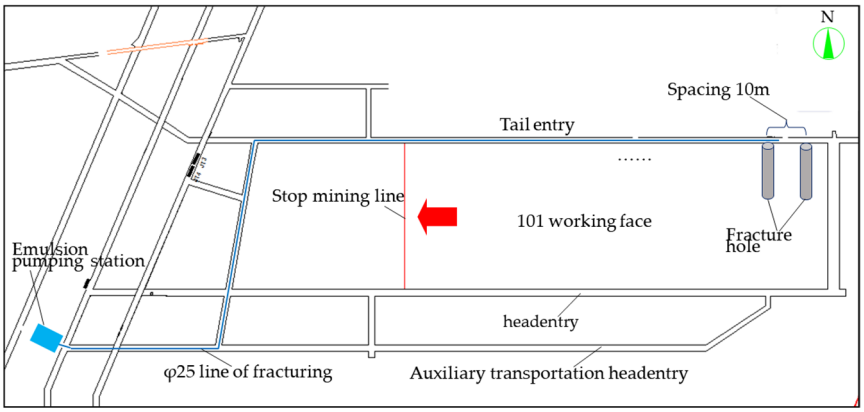



**Figure 3.** Fracturing system layout diagram.

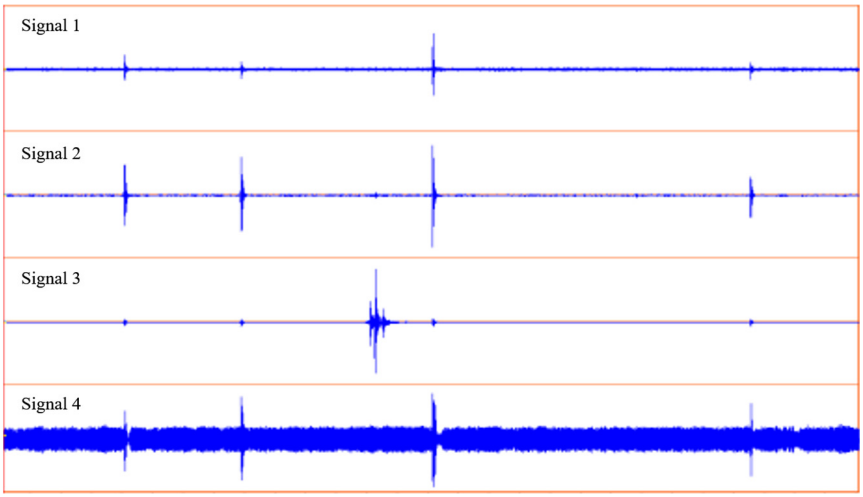



**Figure 4.** Signal change process corresponding to multiple sets of microseismic data during hydraulic fracturing of coal seam.

## 3. Frequency Domain SVD Denoising Method and Principle

### *3.1. SVD Decomposition*

The denoising principle of singular value decomposition (SVD) is that the eigenvalues or singular values are used as the orthogonal basis to enhance the coherent energy and suppress the noise signal [25]. In brief, SVD processes typical seismic signals via multiple channels: (1) the characteristic signal was first extracted from the seismic wave data, which was recorded from a multichannel seismic system; (2) the eigenvalues or singular values for obtaining characteristic signals were solved and further treated as the orthogonal basis to enhance the coherent energy that was present in the seismic wave; and (3) the wavelength separation and denoising were realized by the coherent differences which were directly related to coherent energies [26]. The SVD of the two-dimensional seismic profile matrix $P$ is expressed as:

$$P = USV^T = \sum_{k=1}^{r} \left( \sigma_k U_k V_k^T \right) \quad (1)$$

where $P$ is in $m \times n$ dimensionality in which $m$ and $n$ denote the number of channels and sampling points, respectively; $U$ ($U \in R^{m \times m}$) and $V$ ($V \in R^{n \times n}$) refer to left and right singular matrix (orthogonal). Respectively, $k$ ($k = \min(m, n)$) and $r$ are the ranks of matrix $P$ in the general case of $m << n$; The number of singular values is equivalent to $k$, which

equals the rank of $r$. $S$ is a diagonal matrix generated via the descending order of the $PPT$ (or $PTP$) eigenvalue $\sigma$, $S = diag(\sigma_1, \sigma_2, \ldots, \sigma_k)$:

$$S = \begin{bmatrix} \sigma_1 & & & 0 \\ & \sigma_2 & & \\ & & \vdots & \\ 0 & & & \sigma_k \end{bmatrix}_{n \times n} \tag{2}$$

The singular value ($\lambda_k$) of matrix $PPT$ (or $PTP$) is related to $\sigma_k$, as $\sigma_k = \sqrt{\lambda_k}$, $\lambda_1 \geq \lambda_2 \geq \ldots \geq \lambda_k \geq 0$. In the process of signal reconstruction, the contribution of $\sigma_k$ (i.e., $k$th eigenvalue) to the whole signal is in direct proportion to $\lambda_k$ (i.e., the $k$th singular value). Therefore, $\lambda_k$ or ${\sigma_k}^2$ could characterize the energy magnitude of the seismic signal, in which the contributed faction of $j$th channel $C_j$ can be expressed as:

$$C_j = \frac{\sigma_j^2}{\sum_{i=1}^{k} \sigma_i^2} \tag{3}$$

$C_j$ represents the proportion of energy contributed by the $j$th channel in the total energy. It compares the energy of the $j$th channel with the energy of all channels to determine the contribution of the $j$th channel in the overall context. When $C_j$ has a larger value, it indicates a greater contribution of the $j$th channel to the overall signal. Conversely, when $C_j$ has a smaller value, it suggests a smaller contribution of the $j$th channel to the overall signal. It can be seen that the larger the eigenvalue or singular value of a component, the higher the contributed fraction to the whole seismic signal.

### *3.2. The Denoising Principle of Single Channel SVD*

Unlike multi-channel joint SVD noise reduction processing in the seismic field, conventional microseismic mine monitoring mostly selects 12–36 sensors for real-time monitoring, and the monitoring area and scope are uncertain. Therefore, the correlation between the channels is not strong, and the Hankel matrix constructed from this is not high in dimension. It is difficult to remove noise interference by using the correlation between each channel. Additionally, due to the impact of the geological environment and the requirements for monitoring range and accuracy, the waveforms collected in the mine site often show great differences in multi-channel processing, so conventional multi-channel joint denoising cannot be used. Based on the periodicity present in a single channel [26], we developed a novel SVD method to solve the decomposition and noise reduction of microseismic mine signals. By using SVD, the microseismic signal can be decomposed into several signal components, the eigenvalues of which are ranked via energy amplitude. The effective bandwidth of the eigenvalue was expanded to some extent, and the corresponding frequency was compensated according to energy distribution. At the same time, the signal was reconstructed by removing the eigenvalues mainly corresponding to noise. Compared with the original signal, the $SNR$ of the reconstructed signal has been greatly improved.

In order to realize the SVD, microseismic signals in the single channel should be divided by a fixed length. The microseismic signal was expressed as $X = [x_1, x_2, x_3, \ldots, x_N]$ ($N$ is the sampling site number). For the convenience of SVD analysis, a decomposing matrix, $D_m$, is constructed as:

$$D_m = \begin{bmatrix} x_{(1,1)} & x_{(1,2)} & \cdots & x_{(1,n)} \\ x_{(1\times\tau,1)} & x_{(1\times\tau,2)} & \cdots & x_{(1\times\tau,n)} \\ \vdots & \vdots & & \vdots \\ x_{((m-1)\times\tau,1)} & x_{((m-1)\times\tau,2)} & \cdots & x_{((m-1)\times\tau,n)} \end{bmatrix} \tag{4}$$

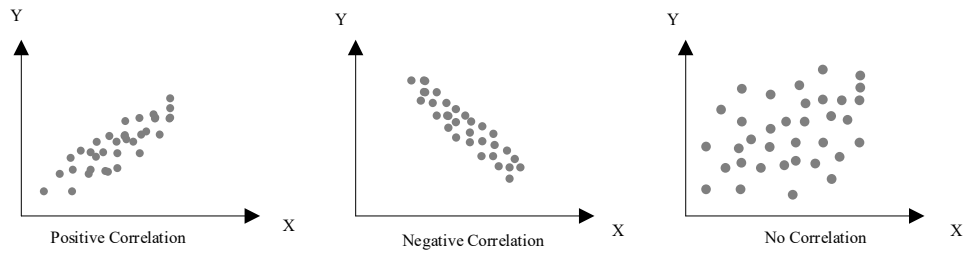
$$D = \overline{D} + N = [U_r U_0] \begin{bmatrix} S_r & 0 \\ 0 & S_0 \end{bmatrix} \begin{bmatrix} V_r^T \\ V_0^T \end{bmatrix} \tag{5}$$

where $m$ is the dimension of matrix reconstruction, $\tau$ is the time delay, and $n$ is the number of sampling points of the signal in each dimension. Matrixes $U$ and $V$ are rotations of the original matrix, while the $S$ matrix is responsible for the degree of matrix linearity (compression), i.e., the higher the matrix linearity, the closer of $\overline{D}$ to $D$ matrix. The SVD denoising processing actually aims to find the optimal approximation of the undisturbed subspace in $\overline{D}$ to $D$, thereby obtaining the best denoising result.

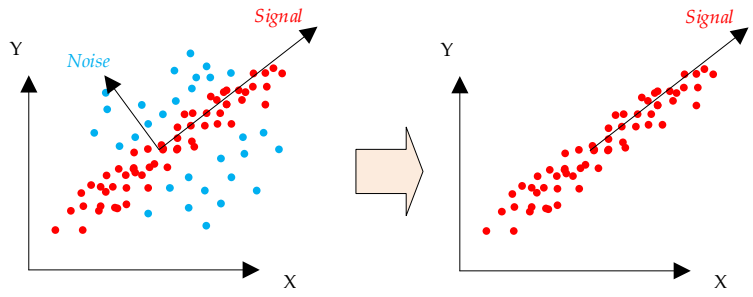
According to the aforementioned analysis, the singular value of the decomposing matrix $D_m$ after SVD processing is combined from three parts as:

$$S_{D_m} = S_W + S_D + S_N \tag{6}$$

where $S_W$, $S_N$, and $S_D$ denote the singular value that corresponds to a strong interference component, random interference, and valid signal, respectively. Therefore, the single-channel microseismic signal denoising by the SVD process aims to retain the valid signal ($S_D$) by setting $S_W = 0$ and $S_N = 0$. Additionally, the denoised microseismic signal can be obtained from the inverse transformation of the SVD process. From Figure 5a, we can see that most of the negative or no correlations will be eliminated, and the better the positive correlation, the more surrounding the true signal itself. The process of setting $S_W = 0$ can be realized by compressing the matrix $D_m$, as illustrated in Figure 5b, in which $S_W$ and $S_N$ are marked with a blue and red color, respectively.




(**a**)




(**b**)

**Figure 5.** Schematic diagram of SVD denoising; (**a**) Signal correlation comparison; (**b**) Signal changes before and after decompression of matrix $D_m$.

Since the singular values were arranged in order from large to small, the original signal was described by several initial characteristic quantities (contributions concentrated) that were extracted from the seismic area. The first several valid singular values in diagonal matrix $S$ were retained, but the singular values of $S_W$ and $S_D$ were still set to 0. Using the optimal settings, the corresponding signal was reconstructed by the inverse process of SVD. It was determined from this process that it is important to optimize the selection of effective singular values in diagonal matrix $S$. The optimization method is interpreted in the next section.

### *3.3. The Denoising Process of the Frequency Domain SVD Method (FSVD)*

The microseismic mine signal is mixed with interference components that are original to the environmental complexity as well as from the transmission process (such as electromagnetic interference). These interference factors will affect signal analysis and processing in the later stage to a great extent. For instance, such interference components can reduce the signal's *SNR*, which increases the difficulty and precision for the onset time pickups of the microseismic wave shape, leading to increased positioning calculation errors. For the microseismic monitoring of the working face, the main frequency range of the effective microseismic signal itself is roughly the same because the monitoring area is basically fixed (within 200 m of the sensor), and the spectrum distribution of the interference component is wide, which provides a basis for the wave field separation of microseismic mine signals. Therefore, the SVD frequency domain denoising technology was used to separate and denoise the microseismic mine waves in this study.

The microseismic mine signal is the superposition of harmonic components in different frequencies. By means of the Fast Fourier transform (FFT), the microseismic signal can be transformed from the time domain to the frequency domain. By treating and analyzing the characteristic frequencies, the reconstructed signal can be obtained from the inverse transformation process of the microseismic signal. This inverse transformation process can be expressed as:

$$\varphi(f) = \int_{-\infty}^{\infty} X(t) e^{-i2\pi ft} \mathrm{d}t \tag{7}$$

$$X(t) = \int_{-\infty}^{\infty} \varphi(f) e^{i2\pi ft} \mathrm{d}f \tag{8}$$

Different from the seismic signal, the microseismic mine monitoring range is generally distributed in a range of 2 km around the sensors. Thus, the common microseismic signal of a rock fracture has a certain regularity in the frequency domain distribution, as the signal interval of the main frequency band is roughly the same, i.e., the microseismic signal spectrum in each channel has a better coherence. Due to the non-stationary and random characteristics of microseismic signals, the invalid interference ought to be removed in order to keep the waveform as complete as possible. The time-frequency denoising method for a single-channel microseismic waveform was developed based on the SVD process, which was modeled in MATLAB®. This method has two procedures, as illustrated in Figure 6: the establishment of a spectrum range for the effective wave and the interference wave and the selection of an appropriate denoising method to suppress the interference wave and highlight the effective wave. The specific process can be summarized as follows:

(1) FFT procedure $X_1(x,t) \rightarrow \varphi(x,f)$: the transformation of the microseismic signal $X_1$ to the frequency domain via FFT (Equation (7)) to obtain the frequency domain signal $\varphi_1$.

(2) Determination of parameters: establishment of the parameters related to SVD for single-channel microseismic signals, such as $\tau$, $k$, and the $n$ and $m$ of the Hankel matrix.

(3) Singular value transformation of SVD ($\varphi_1(x,f) \rightarrow U\sum_1 V$): by means of the parameter values of step (2), the two-dimensional microseismic signal was divided in equal length to construct Hankel matrix $D$, which was performed by SVD (Equation (1)).

(4) Signal reconstruction ($U\sum_2 V^T \rightarrow \varphi_2(x,f)$): analysis of the singular value distribution and establishment of the reasonable reconstruction order, $k$, and singular value ordinal according to the singular value optimization principle.

(5) Inverse FFT ($\varphi_2(x,f) \rightarrow X_2(x,t)$): according to Equation (8), the reconstructed spectrum signal $\varphi_2$ was transformed into the desired target signal, $X_2$, by the inverse Fourier transform.

(6) *SNR* judgment: if the *SNR* did not meet the requirement for the source location, return to (1) step and subsequent performance of steps (2)–(4).

It can be found that the key to single-channel microseismic signal denoising is the selection of parameters during matrix $D_m$ construction, especially for time delay $\tau$. The selection of $\tau$ not only relates to the correlation of data recording in all dimensions of $D_m$

but also affects other parameters' values. That is, the selection of these key parameters is directly related to the effectiveness of the denoising. Methods for the selection and determination of these parameters will be detailed thereinafter.

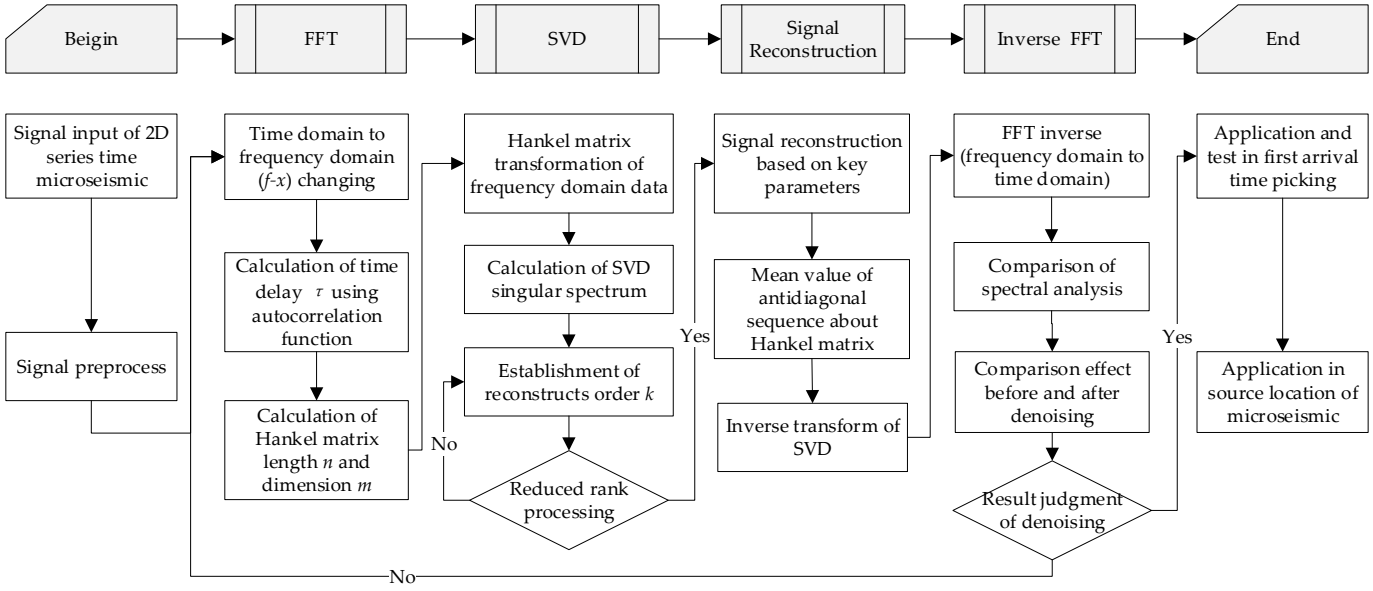



**Figure 6.** Flow diagram of the SVD frequency domain denoising process of microseismic signals.

## 4. Method for Establishing the Key Parameters

The SVD denoising of single-channel microseismic mine signals involves time delay, $\tau$, reconstruction order, $k$, as well as the length, $n$, and dimension, m, of the Hankel matrix. The construction of the Hankel matrix is directly determined by $\tau$, $n$, and $m$. The reconstruction order, $k$, determines the selected singular value for SVD inverse transformation and sets the unselected singular value to 0. At present, there are two common situations in the research of SVD denoising. One realizes the denoising calculation by arbitrarily assigning $m$ and $r$. The other carries out dimensionality reduction (multidimensional signal construction) by using an external model (such as EMD decomposition) followed by SVD denoising. However, according to our results, the EMD denoising would lead to signal distortion, resulting in poor subsequent denoising effectiveness. Thus, it is necessary to optimize and establish the key parameters before the signal-denoising process.

### *4.1. Choice of Time Delay, τ*

The time delay, τ, not only determines the correlation between $D_m$ dimension records but also affects the subsequent values of $k$, $m$, and $n$. The autocorrelation method is a kind of sequence correlation method which can extract the linear correlation between sequences. The $\tau$ for the SVD phase-space matrix construction can be obtained from an autocorrelation function. The reasonable selection of $\tau$ can reduce the correlation between reconstructed time series and retain the dynamic features of the original series as much as possible. The autocorrelation function $R$ of time series $X$ for a single-channel microseismic signal is expressed as:

$$R_{min}(\tau) = \lim_{N\to\infty} \frac{1}{N} \sum_{i=1}^{N} X(n)X(n+\tau) \quad (9)$$

where $N$ is the sampling point of the recorded single-channel microseisms. The delay time, $\tau$, corresponds to the minimum value of $R$ ($R_{min}$).

*4.2. Construction of the Hankel Matrix*

For SVD of microseismic signals, it is necessary to note that all dimensions in the signal matrix have a certain correlation; otherwise the corresponding singular values could not be distinguished clearly. Additionally, SVD denoising will lose effective signals or make them unclean. Therefore, the correlation of internal storage ought to be analyzed before denoising, and then the reasonable parameters of the Hankel matrix are selected to build the phase-space matrix of the single-channel microseismic signal (two-dimensional time series). As reported by Trickett et al., the Hankel matrix can be constructed into a square matrix ($m = n$) [27]. According to Oropeza V et al. [28], the $n$ and $m$ can be calculated as:

$$\begin{cases} n = \frac{N}{2} + 1 \\ m = N - n + 1 \end{cases} \tag{10}$$

Although the $m$ and $n$ can be assigned according to the above equations (Equation (10)), the constructed Hankel matrix has higher dimensions, more eigenvalues, and even higher requirements for calculation time and processing. The $m$ and $n$ could be approximately equal to each other and described by:

$$(m-1) \times \tau + n = N \tag{11}$$

The condition of $m = n$ leads to:

$$m = (N + \tau)/(1 + \tau) \tag{12}$$

*4.3. Reconstructed Order Determination*

According to the SVD theory and best approximation theorem, in order to reduce the effects of noise, the rank of matrix $X$ should satisfy $k < m$. The reconstructed matrix $X$ containing noise signals is a column full rank matrix, $k = m$. Therefore, the essence for denoising of the original signal is to obtain the optimal approximation matrix $X$ of $X'$. Once the singular values matrix $S$ of $X$ is found via SVD, the rank $k$ of matrix $X$ is determined. By further retaining the $1-k$ singular values of the matrix ($\lambda_1, \lambda_2, \ldots, \lambda_k$) and assigning the other $k + 1 \sim m$ singular values ($\lambda_{k+1}, \lambda_{k+2}, \ldots, \lambda_m$) to zero, the optimal approximative matrix $X'$ could be reversely calculated from the inverse SVD process.

It was reported that the key to SVD denoising was the selection of the de-noised order [29]; a lower order could result in missing and lost original signal information. Additionally, a higher order could lead to the retention of overmuch noise information, which pollutes the noise and could not realize denoising. This means that the reconstructed order, $k$, plays a key role in denoising, and it ought to be determined before SVD reconstruction. The conventional methods for $k$ order determination include the threshold method, the trial method, and the singular entropy method. These methods highly depend on the experience value and lead to random denoise effectiveness.

Referring to the study of Xu et al., a concept for singular value energy difference spectrum (SVEDS, E) was introduced to establish the order of reconstructed SVD [30]. $E$ characterizes the adjacent singular values in changing of energy and can be calculated as:

$$E(i) = (\lambda_i^2 - \lambda_{i+1}^2)/({\lambda_{max}}^2 - {\lambda_{min}}^2) \tag{13}$$

where $i$ denotes $i$th SVEDS, $i = 1, 2, \ldots$ and $k-1$; $\lambda_i$ is the $i$th singular value whose minimum and maximum are $\lambda_{min}$ and $\lambda_{max}$, respectively.

## 5. Analysis of Experimental Results

In order to verify the effectiveness of the SVD denoising method for single-channel signals, a microseismic event measured at a mine site in Shandong province, China, was taken as an example (time: 10 June, 20:13:42). Figure 7 shows the waveform of this typical microseismic event, which was monitored with the following parameters: sampling

frequency, 1000 Hz; continuous collection cache with subsequent collection and interception by STA/LTA, 15 min; velocity type sensor with a characteristic frequency of 50~5 kHz and sensitivity of 30 V/g; and collection frequency range, 0~1000 Hz. The microseismic sensor was embedded in the coal seam (20~45 m from the pore mouth) to collect the microseismic signals of coal rock fracture.

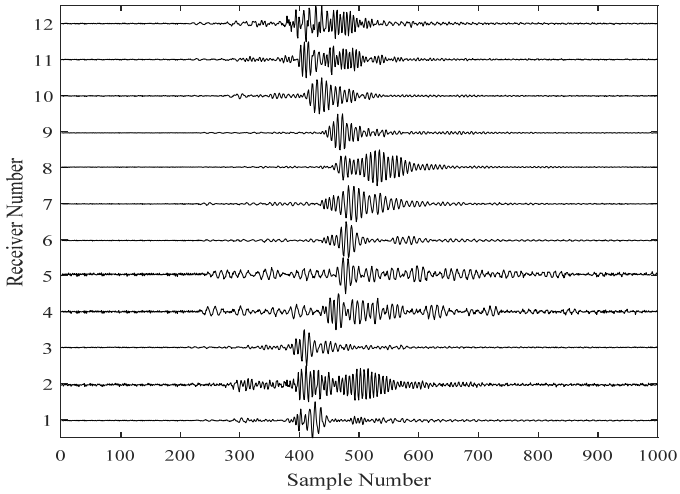



**Figure 7.** Waveform of a typical microseismic event.

### *5.1. Select Key Parameters*

According to the selection methods for key parameters in Section 4, the microseismic field events in Figure 7 were studied. At the same time, taking single channel 9# as an example, how to obtain each key parameter and how to judge the effect effectively after denoising is introduced.

#### 5.1.1. Calculation Delay Time (τ)

In view of the characteristics of the 9# single channel, we used the autocorrect function of MATLAB® to calculate the autocorrelation coefficient of the signal. The corresponding calculation result is shown in Figure 8 and Table 1. According to Section 2.1 and Equation (9), the delay time $\tau = 9$ was selected corresponding to the minimum $R$ ($R = 0.0049$).

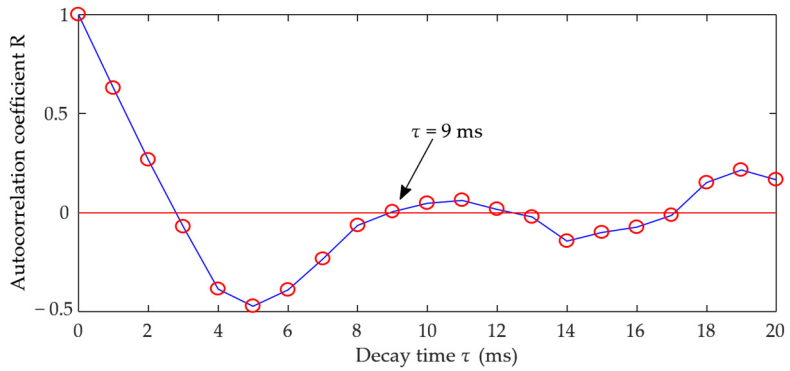



**Figure 8.** Result of calculated $\tau$ and its autocorrelation coefficient, $R$.

**Table 1.** Result of calculated $\tau$ and its autocorrelation coefficient, $R$.

| ID | $\tau$ | $R$ | ID | $\tau$ | $R$ |
|---|---|---|---|---|---|
| 1 | 0 | 1 | 12 | 11 | 0.0623 |
| 2 | 1 | 0.6287 | 13 | 12 | 0.0169 |
| 3 | 2 | 0.2667 | 14 | 13 | −0.0210 |
| 4 | 3 | −0.0713 | 15 | 14 | −0.1430 |
| 5 | 4 | −0.3860 | 16 | 15 | −0.1000 |
| 6 | 5 | −0.4724 | 17 | 16 | −0.0725 |
| 7 | 6 | −0.3896 | 18 | 17 | −0.0132 |
| 8 | 7 | −0.2335 | 19 | 18 | 0.1527 |
| 9 | 8 | −0.0638 | 20 | 19 | 0.2156 |
| 10 | 9 | 0.0049 | 21 | 20 | 0.1663 |
| 11 | 10 | 0.0472 | | | |

#### 5.1.2. Construction of the Hankel Matrix

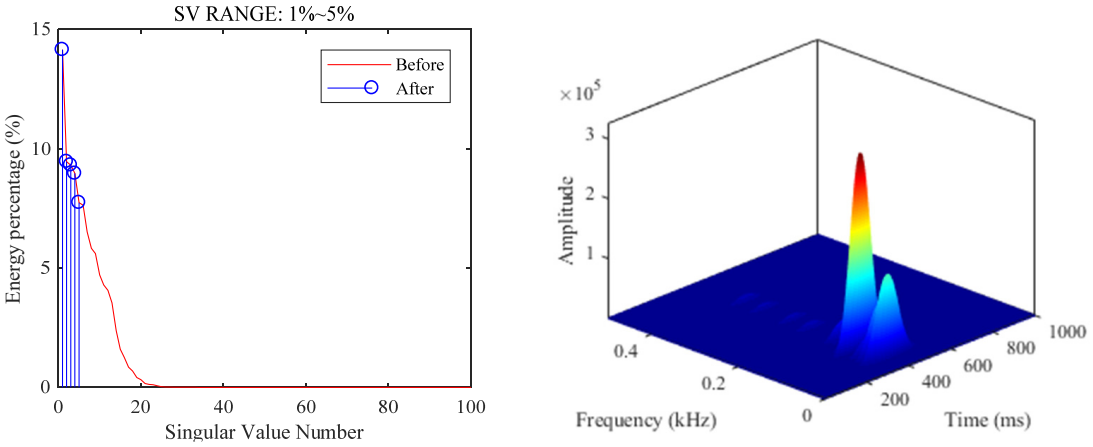
According to the method detailed in Section 5.1.1, the value of $\tau$ = 9 was substituted into Equation (12), and the $m$ and $n$ were solved as $m$ = 100 and $n$ = 109. Once these key parameters of the Hankel matrix were constructed, the SVD for single-channel microseismic signals could be realized. The next step aimed to select a reasonable SVD reconstruction order, i.e., the singular value corresponding to the effective signal.

#### 5.1.3. Establishment of Reconstructed Order

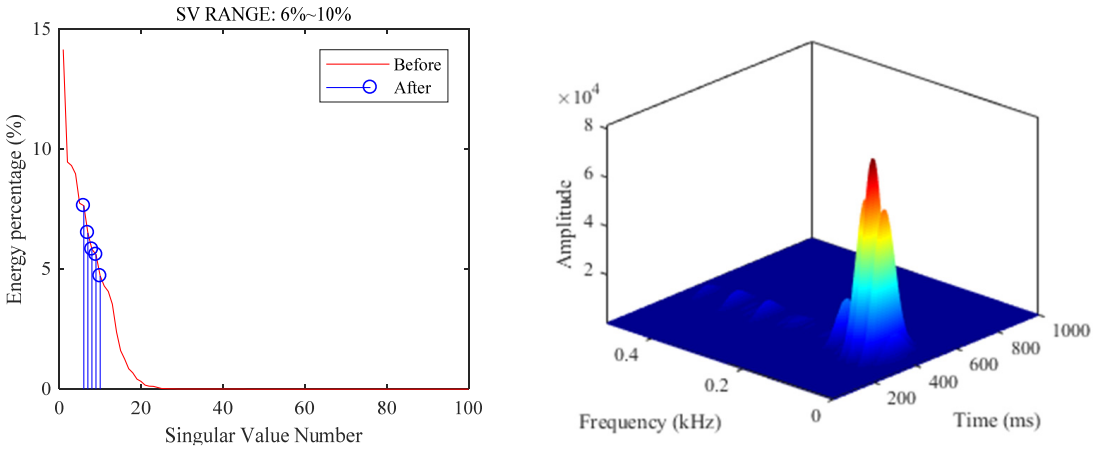
In order to illustrate the rationality of the selected reconstruction order, the signal was reconstructed according to different singular value ranges to observe the contributed fraction of each singular value to the original microseismic signal. The main frequency of microseismic mine signals was concentrated in the range of 50~200 Hz, which was relatively strong in noise energy and wide distribution. By performing SVD of this frequency spectrum, the original signal's energy spectrum was mainly distributed in the first 20 signals, which were treated as an objective serial.

The as-constructed Hankel matrix was decomposed by FSVD, where the regular singular value sequences were selected and reconstructed according to the rule that singular values of ordinal numbers, 1~5, 6~10, 11~15, 16~20, and 21~25, were selected respectively. The spectrum characteristics of FSVD singular value energy distribution and the corresponding reconstructed signals were obtained as illustrated in Figure 9, where the red and blue curve on the left-hand side denotes the energy proportion and singular value number, respectively; the right-hand side is the spectrum diagram of the reconstructed signal by selecting the singular value sequence. It can be found that the features of the reconstructed signal (by selecting different sequences, i.e., order numbers) were quite different: the signal still retained its waveform (Figure 9a–c), while noise was in a dominant role (Figure 9d,e).

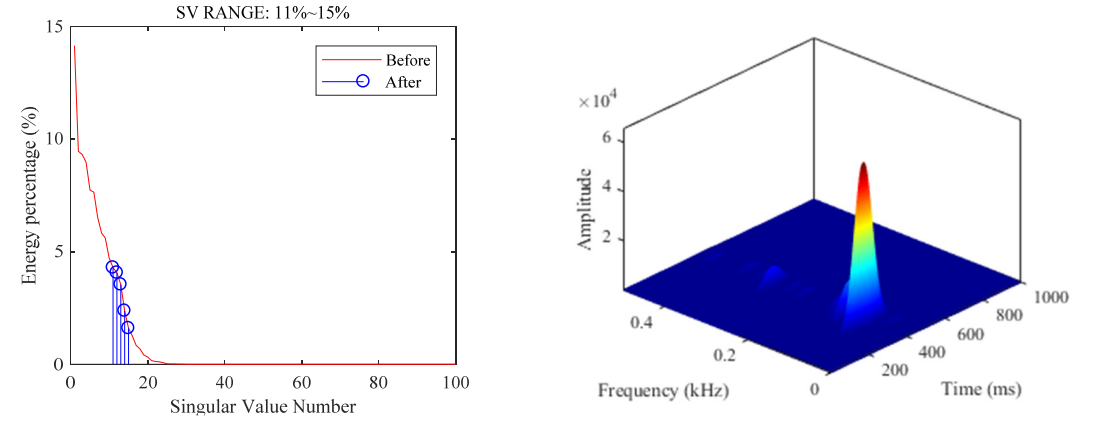
The noise in Figure 9a has been effectively suppressed but with more details lost, which is mainly attributed to the incomplete singular values selected. From Figure 9b, the singular values of the series had both effective components and interference components that belong to a transitional zone. However, the spectrum features of Figure 9d,e showed that SVD had little influence on the waveform's effective components. Thus, ordinal numbers of 1~15 can be treated as the effective singular value sequence. It can also be found from the final denoising results that Figure 9a–c shows the best denoising effectiveness: the main frequency components were effectively protected, the suppressed noise at the bottom was clean, and the starting point was obvious and remained at the original state.




(**a**)

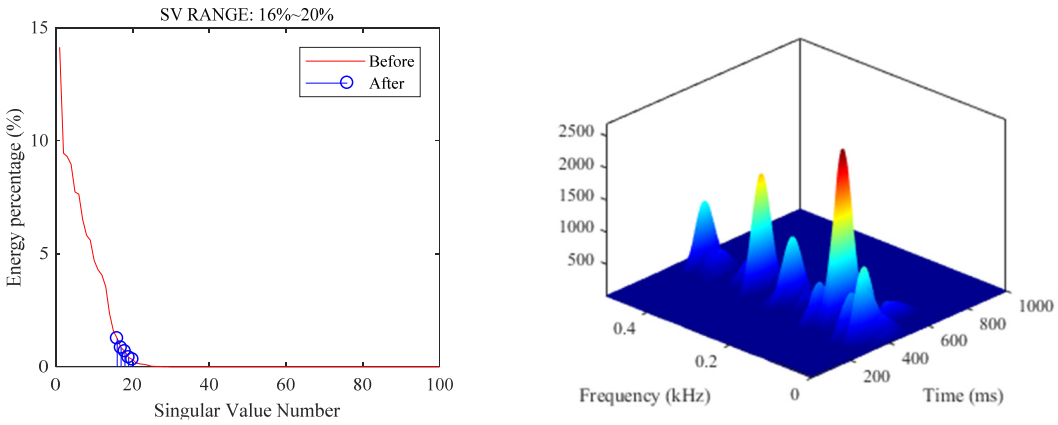



(**b**)

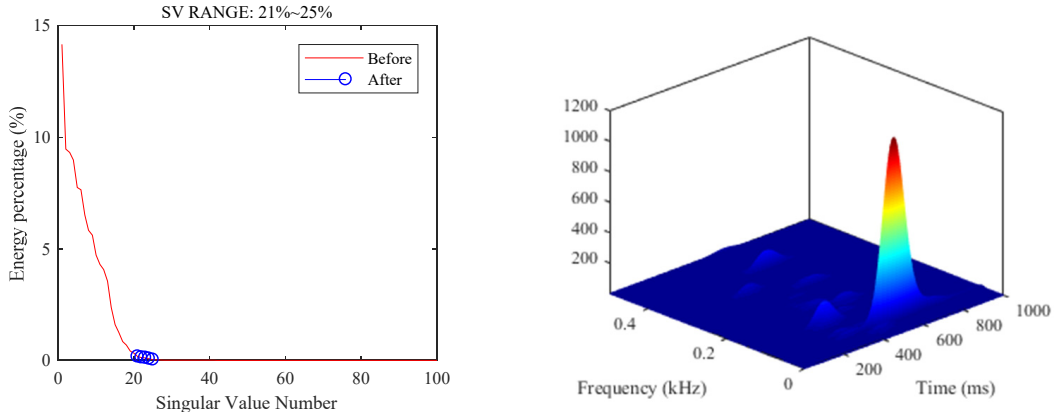



(**c**)

**Figure 9.** *Cont.*




(**d**)




(**e**)

**Figure 9.** Different singular value ranges corresponding waveform features; (**a**) 0~5; (**b**) 6~10; (**c**) 11~15; (**d**) 15~20; and (**e**) 20~25. The red curve on the left is the proportion of energy, and the blue line corresponds to the singular value number. On the right is the spectrogram of the signal reconstructed by the selected singular value sequence. The brighter color from bottom to top indicates that the energy is larger in the corresponding time-frequency range.

### *5.2. Spectrum Analysis and Comparison at Different SNRs*

In order to illustrate the effectiveness of the denoising method for the microseismic signal, channels 5# and 12#, which represented high and low *SNR*, respectively, were taken as examples. As shown in Figure 10, we compared the waveform and spectrum changes before and after denoising. Figure 10 illustrates that noise from the microseismic signal had been effectively suppressed, and the time-frequency distribution range was more concentrated, while the corresponding noise had been obviously suppressed. It was evident that the microseismic signal with the 600~800 ms frequency components was removed, and the 320 Hz band was weakened after de-nosing, which was quite different from the frequency before denoising (widely distributed at 0~400 Hz, continuously ranged from 200~800 ms), as shown in Figure 10a. Figure 10b shows that the removal effectiveness of a low *SNR* signal was more obvious, especially in the 300~400 Hz range, whose waveform noise was preferably suppressed. Thus, our method could not only suppress and remove the abnormal frequency components but also retain the main components of the original signal.

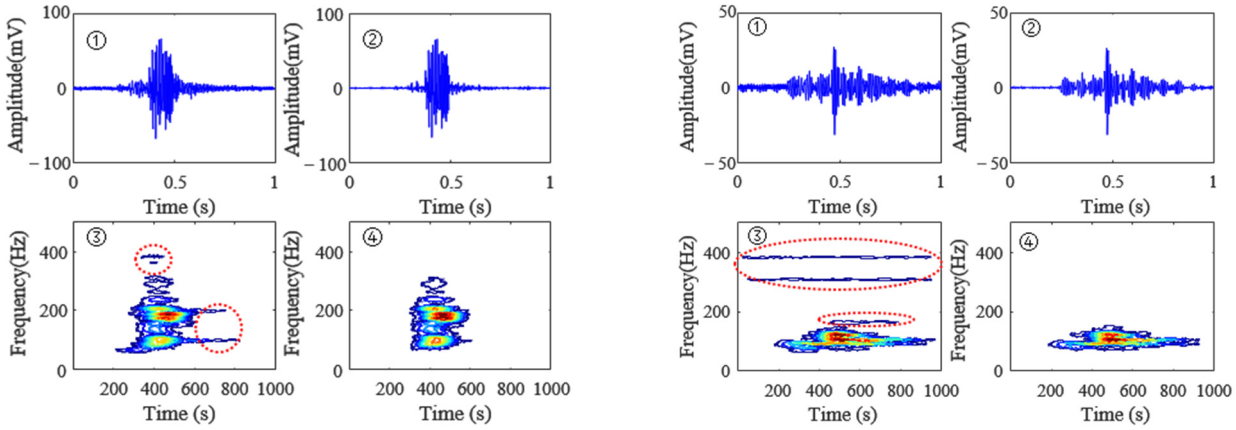



**Figure 10.** Analysis of noise removal effect of FSVD under different *SNR*: (**a**) Results of high *SNR* signal before and after denoising(channels 5#): ① The original signal before denoising, ② the signal after FSVD denoising, ③ is the amplitude distribution of the original signal in the time-frequency domain, the larger the amplitude, the darker the color. ④ is the amplitude distribution of the signal after denoising in the time-frequency domain. (**b**) Results of low *SNR* signal before and after denoising(channels 12#): ① The original signal before denoising, ② the signal after FSVD denoising, ③ the energy distribution of the original signal in the time-frequency domain, and ④ the energy distribution of the signal after denoising in the time-frequency domain. The red circle represents the energy corresponding to the noise removed in its time-frequency range after FSVD denoising.

### *5.3. Comparison and Analysis of the Effect of Noise Reduction by Various Methods*

In order to verify the feasibility of our FSVD method, the Bandpass filter was considered for the characteristics of this waveform with the Bandpass upper and lower limit of 10 Hz and 200 Hz, respectively. SVD was used to carry out a comparative analysis, which contraposed the denoising effectiveness and difference before and after denoising. Figure 11 shows the FFT results after denoising, whose waveforms, as well as removal noise, are given in Figure 12. As illustrated in these Figures, the Bandpass filter, SVD, and FSVD methods could effectively suppress the interference of strong noise, especially the high-frequency part. The basic frequency characteristics of the vibration waveform were also preserved. Bandpass filter is widely used in denoising processing of seismic signals. However, as shown in Figures 11 and 12, Bandfilter could preserve all features of the signal in the designated frequency band range. The components outside of the band range were removed, and the low-frequency part was even prone to distortion. The SVD method was less effective compared with the FSVD method in the aspect of waveform detail processing. However, it was obvious that the spectrum curve obtained by FSVD denoising was smoother than the Bandfilter and SVD methods. By contrast, Bandfilter excessively relied on setting the frequency of the upper and lower limits. The corresponding mandatory setting of the frequency domain space easily caused the loss of effective signal components and failed to filter out interference components within the domain frequency. The SVD method focused on the compression of the signal's time domain, but it was not enough to detail the signal (especially obvious in the frequency range of 50~200 Hz), leading to signal or waveform distortion in the predominant frequency band. Compared with the SVD method, the FSVD method retained the effective signals better in both the high- and low-frequency ranges and could effectively suppress the interference noise in the predominant frequency band.

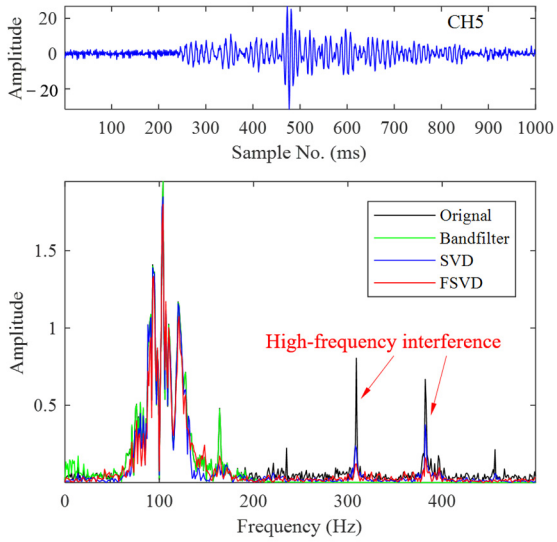
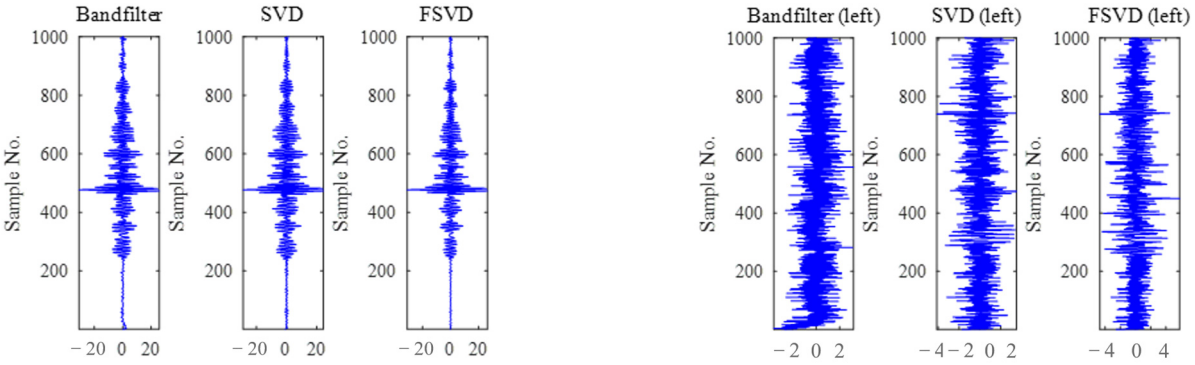



**Figure 11.** Three methods, Bandfilter, SVD, and FSVD, were used to compare the spectrum distribution of single channel signals after denoising.




(**a**) (**b**)

**Figure 12.** Comparison of the denoising effect for three methods: Bandfilter, SVD, and FSVD. (**a**) The denoising results of three methods: Bandfilter, SVD, and FSVD. (**b**) Noise removal by three methods: Bandfilter, SVD, and FSVD.

### *5.4. Performance Analysis*

The microseismic signal before and after denoising could be quantitatively described by indexes of *SNR*, energy percent (*ESN*), root mean square error (*RMSE*), and signal smoothness (*STI*) as follows:

$$SNR = 10\lg\left\{\sum_{n=1}^{N} S_n^2 / \sum_{n=1}^{N}\left[\left(S_n - \hat{S}_n\right)^2\right]\right\} \tag{14}$$

$$ESN = \sum_{n=1}^{N} \hat{S}_n^2 / \sum_{n=1}^{N} S_n^2 \tag{15}$$

$$RMSE = \sqrt{\sum_{n=1}^{N}\left[\left(S_n - \hat{S}_n\right)^2\right]/N} \tag{16}$$

$$STI = \sum_{n=1}^{N-1}\left(\hat{S}_{n+1} - \hat{S}_n\right)^2 / \sum_{n=1}^{N-1}\left(S_{n+1} - S_n\right)^2 \tag{17}$$

where $S_n$ and $\hat{S}_n$ denote microseismic signals before and after denoising, respectively; $N$ is the sampling point of the signal. The four calculated indexes (i.e., *SNR*, *ESN*, *RMSE*, and *STI*) for Bandfilter, SVD, and FSVD are compared in Table 2. In this table, it can be found that the *SNR* for all channels had been obviously changed by >10 db (except for the 4.47 db change for CH3 using the SVD method), indicating that the Bandfilter, SVD, and FSVD methods could improve the *SNR* of the microseismic signal to a great extent. The *ESN* index characterizes the integrity of signal energy, i.e., a larger *ESN* value illustrates the integration of original signal features. The Bandfilter method gave a higher *ESN* value (higher than 0.9) than SVD and FSVD. The *RMSE* of the three methods showed similar variation trends, indicating that the effect deviation of these methods was not large after denoising. However, significant differences were found in the *STI* index. The Bandfilter algorithm showed the worst *STI*, while SVD was close to FSVD, and FSVD had a better effect (distributed in the range of 0~0.71). On the aspect of *SNR*, the highest *SNR* still reached 18.24 db, 15.01 db, and 10.08 db, even for the seriously polluted channels 2, 4, and 10, respectively.

**Table 2.** Comparison of denoising results using different methods.

| ID | Bandfilter | | | | SVD | | | | FSVD | | | |
|---|---|---|---|---|---|---|---|---|---|---|---|---|
| | **SNR** | **ESN** | **RMSE** | **STI** | **SNR** | **ESN** | **RMSE** | **STI** | **SNR** | **ESN** | **RMSE** | **STI** |
| CH1 | 29.41 | 0.92 | 1.42 | 0.02 | 10.48 | 0.52 | 1.43 | 0.04 | 22.95 | 0.88 | 1.57 | 0.03 |
| CH2 | 26.81 | 0.93 | 0.87 | 9.81 | 24.51 | 0.86 | 1.57 | 0.22 | 18.24 | 0.73 | 1.09 | 0.05 |
| CH3 | 41.69 | 0.98 | 1.34 | 8 | 4.47 | 0.31 | 1.69 | 0.01 | 12.18 | 0.68 | 1.49 | 0 |
| CH4 | 30.65 | 0.96 | 0.81 | 5.74 | 18.97 | 0.71 | 0.78 | 0.79 | 15.01 | 0.67 | 0.83 | 0.01 |
| CH5 | 27.69 | 0.95 | 2.66 | 11.64 | 26.64 | 0.9 | 1.75 | 1.89 | 23.37 | 0.8 | 2.55 | 0.46 |
| CH6 | 42.92 | 0.99 | 0.73 | 0.08 | 35.62 | 0.9 | 0.25 | 0.15 | 30.62 | 0.93 | 0.48 | 0 |
| CH7 | 47.71 | 0.99 | 0.3 | 12.86 | 37.58 | 0.96 | 0.31 | 1.06 | 24.07 | 0.88 | 0.23 | 0.71 |
| CH8 | 44.32 | 1 | 1.13 | 0.92 | 57.04 | 1 | 1.77 | 0 | 51.98 | 0.99 | 2.12 | 0.11 |
| CH9 | 35.13 | 0.97 | 2.25 | 0.11 | 42.76 | 0.97 | 2.19 | 0.49 | 37.64 | 0.97 | 2.16 | 0.01 |
| CH10 | 44.39 | 0.99 | 1.76 | 1.83 | 12.19 | 0.61 | 1.87 | 0.02 | 10.08 | 0.62 | 1.67 | 0 |
| CH11 | 34.88 | 0.9 | 1.91 | 1.07 | 36.34 | 0.96 | 1.99 | 0.75 | 34.43 | 0.95 | 1.9 | 0.68 |
| CH12 | 20.71 | 0.76 | 1.41 | 0.28 | 31.2 | 0.93 | 1 | 0.17 | 28.21 | 0.91 | 1.16 | 0.04 |

In general, there are many random noises in the microseismic signal, which have a wide spectrum distribution and no coherence. The conventional methods can only weaken part of the noise. For example, Bandfilter cannot eliminate the noise of the main frequency band and also loses the effective signal components of high- and low-frequency bands. The FSVD method can retain the effective signal in high- and low-frequency bands and suppresses interference noise of the predominant frequency band. Although the Bandfilter method could retain the detailed features and energy of signals, the signal changes before and after processing were not obvious, which was mainly reflected in the *STI* (Table 2). At the same time, the Bandfilter method causes distortion in low-frequency or high-frequency parts, as shown in Figure 13.

It is necessary to suppress the noise completely before picking the first arrival times (FirAT) since factors (such as too much bottom noise) will affect the picking effectiveness and the accuracy of final arrival times (FinAT). The method only using the Bandfilter or SVD method did not show the desired effectiveness for first arrival times pickup. The protection of high- and low-frequency components had been weakened by the Bandfilter method; the smoothness of the wave curve could not be guaranteed by SVD (i.e., the burr part of the signal could not be eliminated effectively). Although the FSVD method had disadvantages in *SNR* and *ESN*, the *RMSE* was small. FSVD can not only retain the original signal characteristics better but also satisfy the denoising effectiveness well. Thus, it can be perorated that the FSVD showed the best effectiveness on microseismic signal denoising, which is conducive to the picking of the FinAT.

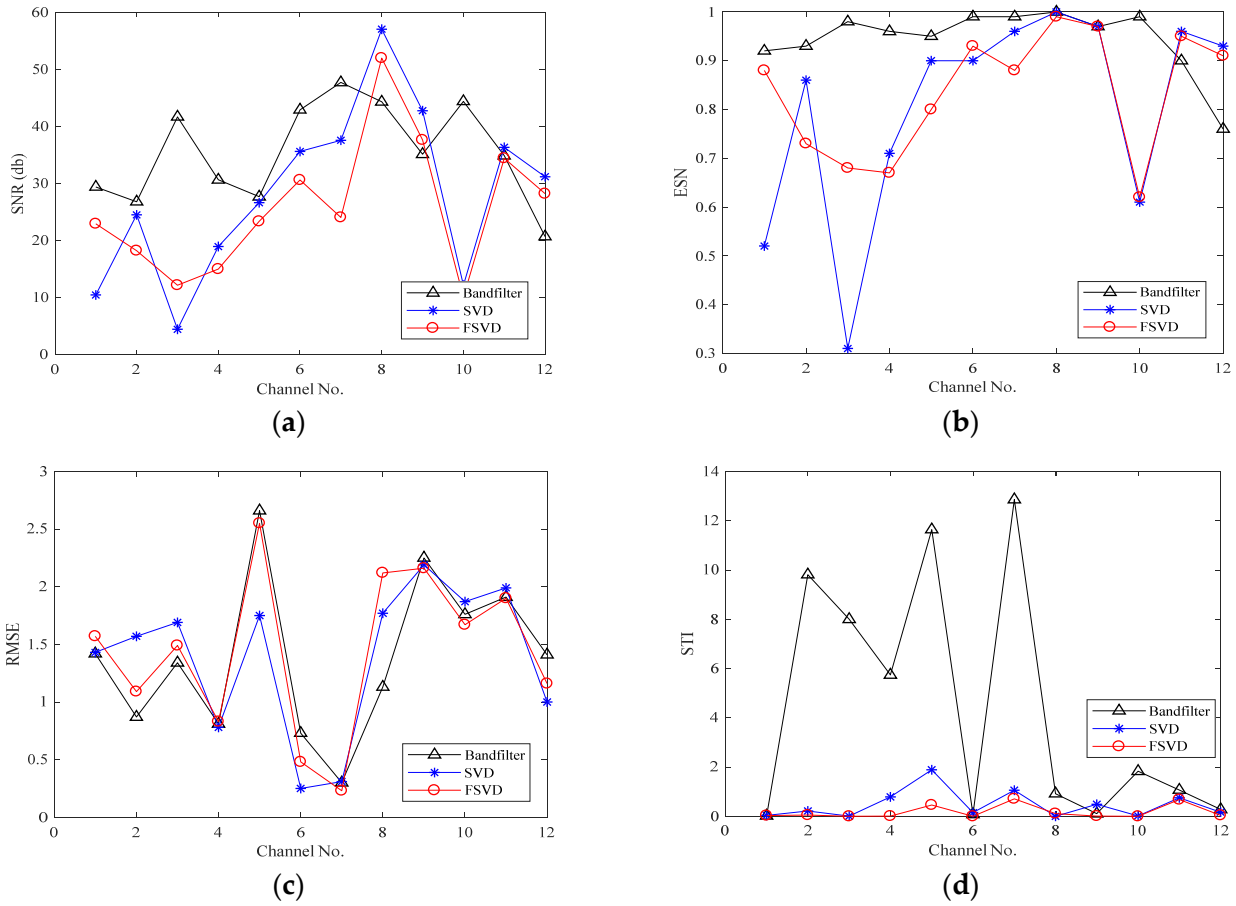


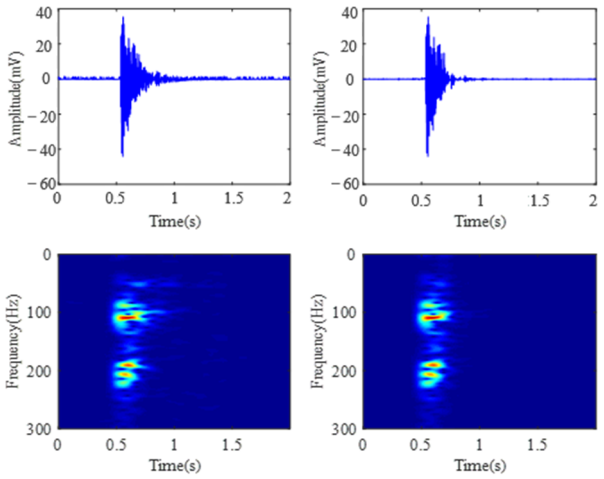

**Figure 13.** Performance evaluation of three denoising methods: Bandfilter, SVD, and FSVD: (**a**) *SNR*; (**b**) *ESN*; (**c**) *RMSE*; and (**d**) *STI*.

## 6. Result

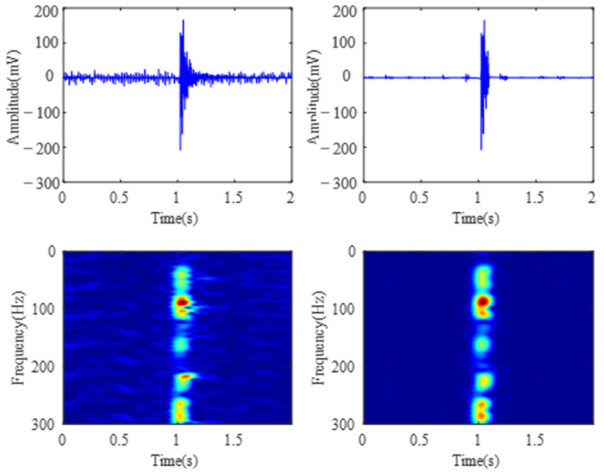
### *6.1. Denoising Effectiveness of Microseismic Signals*

The denoising effect of microseismic mine signals directly affects waveform classification recognition, time picking, location calculation, and attribute mining. There are many kinds of microseismic signals in mines. Typical microseismic signals include electromagnetic interference signals, blasting vibration signals, rock fracture microseismic signals, and drilling signals. In this study, three representative microseismic mine signals were selected to verify the FSVD noise reduction method.

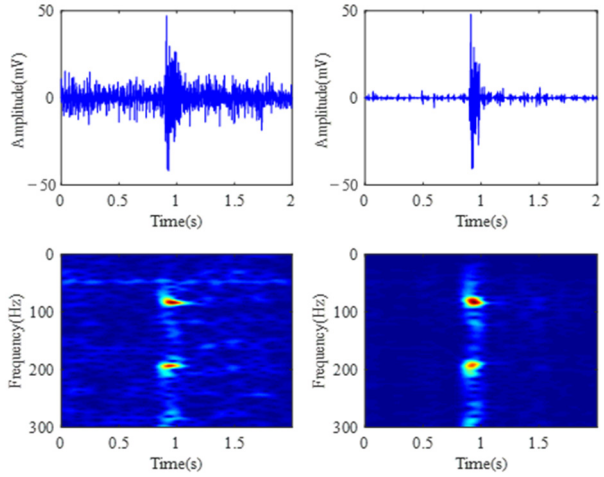
Figure 14 shows that the blasting vibration signals had two peaks in the frequency domain, 100 Hz and 200 Hz. After denoising, the signal spectrum was more concentrated, and the bottom noise was effectively suppressed. The background noise amplitude of the coal cannon vibration signal was large, where the FirAT signal was submerged in the bottom noise. This indicated that the signal noise was effectively eliminated, but the energy in the region outside the main frequency band was also eliminated, leading to a more concentrated frequency. The *SNR* of the roof falling signal was low, and it was completely submerged in the bottom noise at the beginning of the FirAT. The arrival time of this kind of signal cannot be effectively picked up manually. After denoising, the bottom noise of the signal was obviously suppressed, and it can also be seen from the spectrum that the signal was more "clean" after denoising, and the waveform characteristics were more obvious.




(**a**)




(**b**)




(**c**)

**Figure 14.** Comparison of the effect of three microseismic signals before and after denoising: (**a**) blasting vibration signal; (**b**) coal cannon vibration signal; and (**c**) roof falling vibration signal.

### *6.2. Experimental Verification of the Time Pickup of the Denoised Signal Based on FSVD*

The positioning accuracy of a microseismic signal relies on the pickup precision of the signal's FinAT, which is based on the high *SNR* signal. The denoising quality of the signal directly affects the pickup accuracy of FirAT. Therefore, we used the manual pickup

as a reference to study the waveform of the microseismic signal at FinAT by using the FSVD method. For the pickup of the FinAT-regarded microseismic signal (Figure 15), the denoising effectiveness of the FSVD method was evaluated by ER, MER, WFM, PAI-S/K, and IAIC, whose results are shown in Figures 15 and 16. As shown in Figures 15 and 16, it can be found that the *SNR* had been changed to a great extent after FSVD denoising and became more obvious than in the SVD and Bandfilter methods. Finally, five typical picking methods for FinAT were used to verify the above methods of the denoising results and effectiveness. The results show that the picking error of FSVD was better than in SVD and Bandfilter, and the error picking by the IAIC method was obviously better than in other methods. Especially the average picking error of IAIC after FSVD denoising (12.17 ms) was much better than in SVD (28.03 ms) and Bandfilter (31.0 ms).

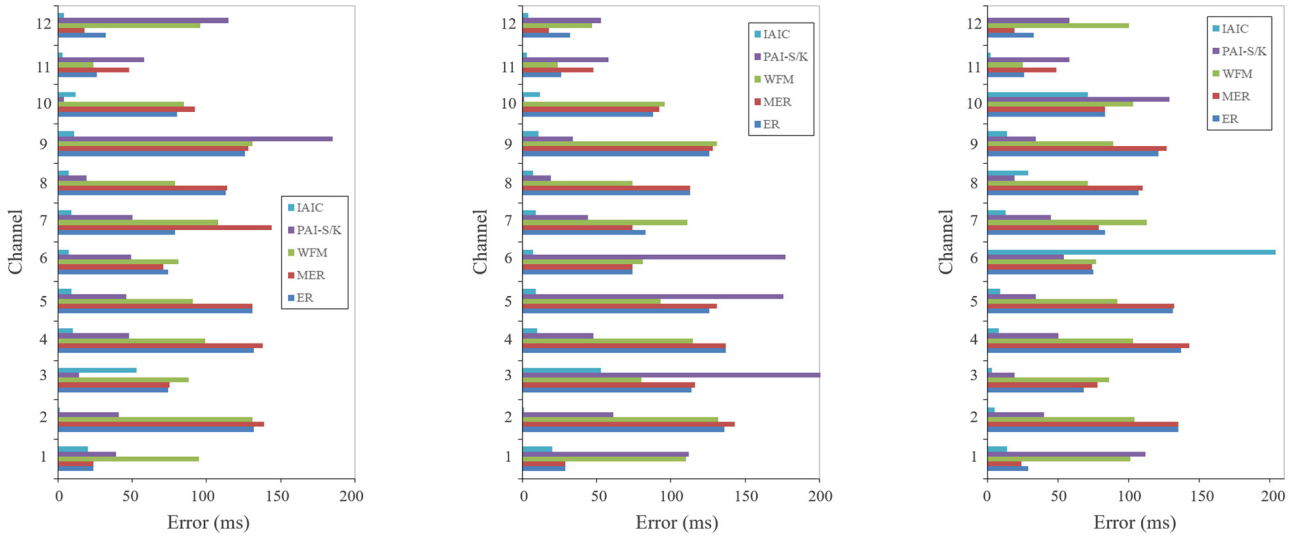



**Figure 15.** Comparison of error between the manual picker and automatic picker using five common picking methods: (**a**) FSVD; (**b**) SVD; and (**c**) Bandfilter.

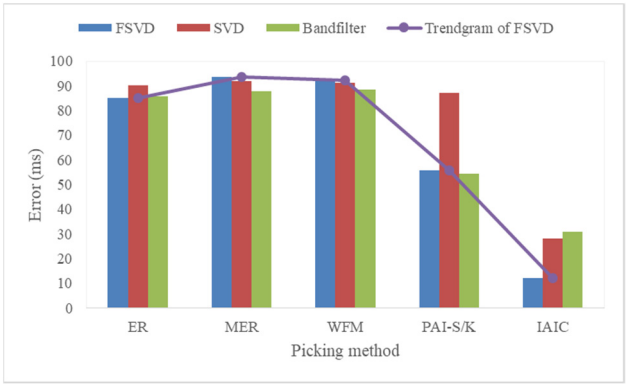



**Figure 16.** Difference between five common picking methods (including ER, MER, WFM, PAI-S/K, and IAIC methods).

As shown in Figure 17, the microseismic waveform after FSVD processing (blue color) is a typical pickup result of FinAT. It can also be found that the *SNR* had been changed to a great extent after FSVD denoising, and the initial jump position of the signal became more obvious, indicating that the pickup of FinAT was accurate via FSVD processing. Additionally, as compared in Figure 17, the results obtained from IAIC (red color) are more similar to those obtained from the manual pickup, indicating that the IAIC algorithm could

satisfy field application requirements. Meanwhile, it can be found that the IAIC method has the characteristic of a sensitive, accurate, and fast speed, especially for the low *SNR* and minor amplitude, which cannot be seen.

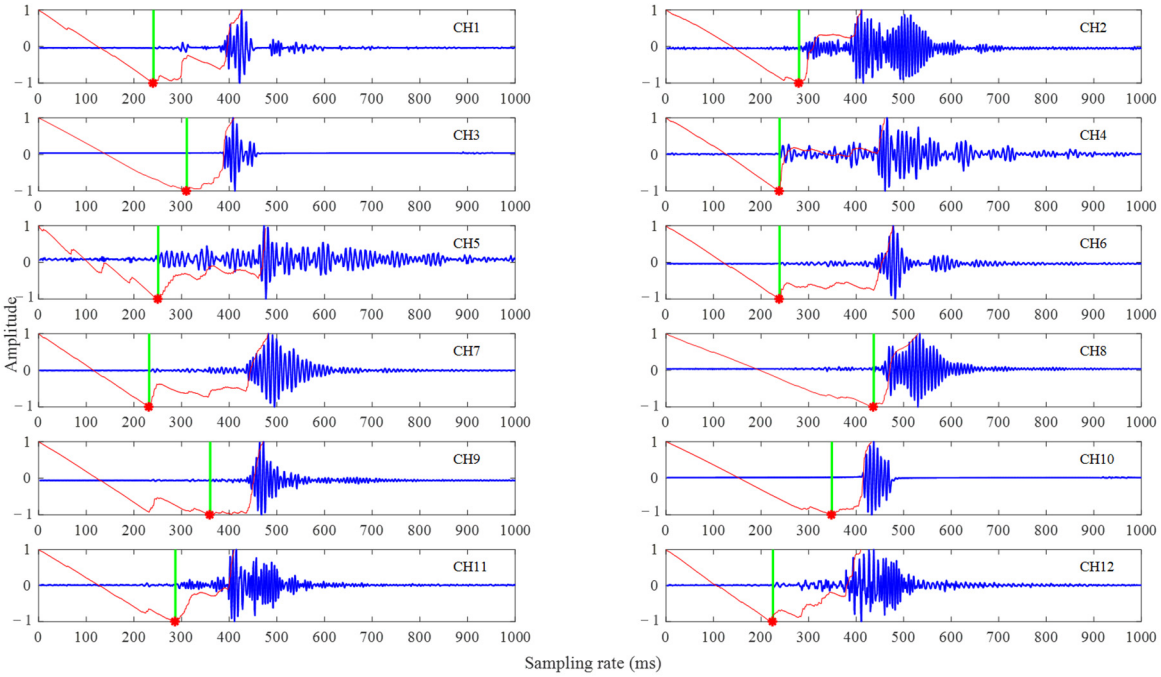



**Figure 17.** Automatic picker of FSVD denoising signals using the IAIC method (the red curve is the characteristic curve of IAIC picking, the abscissa point corresponding to the green line is the initial picking time, and the blue curve corresponds to the microseismic signal).

From the final results, the pickup precision of each channel was greatly improved after FSVD denoising. The average error derived from denoising (6.7 ms) was lower than that before denoising (32.0 ms). The *SNR* of the CH6, CH8, and CH10 signal noises with large errors was relatively low, which was attributed to the fact that signal noise affects the accurate selection of the FinAT. Thus, it can be perorated that the pickup time after denoising was closer to the manual pick. That is, the pick accuracy could be guaranteed by the FSVD method, which provides a foundation for subsequent positioning calculations.

## 7. Discussion

Therefore, taken together, the FSVD denoising method proposed in this study can improve the accuracy of automatic pickup to a certain extent. This denoising method can even replace the manual pickup method because of its high precision. To a certain extent, it can solve the problem of the pickups of the FirAT for mine-seismic waves, providing a premise for the micro-seismic locating calculation. However, some contents need to be further improved to consummate the FSVD method for microseismic signal processing, such as the identification of effective waveform and the selection and judgment of microseismic events in the external field.

## 8. Conclusions

Considering the low *SNR* characteristics of microseismic mine waveforms, a single channel frequency domain SVD method was proposed to denoise the microseismic signal. The following conclusions can be drawn from the above analysis:

(1) On the basis of previous studies, a single-channel FSVD noise reduction method for microseismic mine signals was proposed. The essence of this method was to transform the microseismic signal into the frequency domain via SVD to achieve the aims of signal feature enhancement and interference noise suppression from the frequency domain perspective.

This novel method can avoid the serious loss of effective signals and effectively realizes wavelength separation and noise removal.

(2) Based on the analysis of single-channel waveform characteristics, the novel FSVD method was developed by coupling the fast Fourier transform (FFT) and SVD via decomposed matrix Dm construction. This method can effectively realize the denoising of single-channel waveforms for microseismic mines by establishing the time delay, $\tau$, reconstructed order, $k$, and Hankel matrix.

(3) Comparisons between Bandfilter, SVD, and FSVD methods were carried out via *SNR*, *RMSE*, *ESN*, and *STI* indexes. Results show that the Bandfilter method could detail the microseismic signal features and lead to an oversized bottom noise signal, which was unable to pick up the starting point of the FirAT accurately. The FSVD and SVD methods could improve *SNR* and maintain a sufficient signal energy similar in the *SNR*, *RMSE*, *ESN*, and *STI* indexes. The FSVD method was favorable in ensuring the smoothness of waveform (*STI*) over Bandfilter and SVD.

(4) Through field verification, the FSVD method could effectively remove the noise of several typical waveforms. The FSVD method could preserve the waveform characteristics well, and the initial jump point was obvious. This method could effectively improve picking accuracy and meet the needs of field application. It could more accurately identify the geological information in the microseismic signal, help to understand the mechanical properties of underground rocks and coal seams, further optimize the mining scheme, and improve the mining efficiency. This is of great significance for mine safety monitoring, disaster warning, and resource exploitation.

**Author Contributions:** Conceptualization, Q.Z. and Q.L.; methodology, Q.Z., Q.L. and Y.L.; software, Q.Z. and L.S.; validation, Y.L., L.G. and D.W.; formal analysis, Q.Z., L.S. and L.G.; investigation, L.S., L.G. and D.W.; resources, Q.L. and Y.L.; data curation, L.S. and L.G.; writing original draft preparation, Q.Z. and L.S.; writing review and editing, L.S., Q.L. and L.G.; visualization, L.G. and D.W.; supervision, Q.Z. and Q.L.; project administration, Q.Z.; funding acquisition, Q.Z., L.S. and Q.L. All authors reviewed the manuscript. All authors have read and agreed to the published version of the manuscript.

**Funding:** This research was funded by the Central Government Guides Local Science and Technology Development Fund Project, grant number 216Z5401G, Guizhou Province High-Level Innovative Talent Training Program Funding Project, grant number [2019]5675, the Fundamental Research Funds for the Central Universities, grant number 3142021002, Education Department of Hebei Province Graduate Student Innovation Ability Training Funding Project, grant number CXZZSS2023183, and the Scientific Research Program of Colleges and Universities in Hebei Province, grant number Z2020124.

**Institutional Review Board Statement:** Not applicable.

**Informed Consent Statement:** Not applicable.

**Data Availability Statement:** The data used to support the findings of this study were supplied by Quanjie Zhu under license and so cannot be made freely available. Requests for access to these data should be made to Quanjie Zhu (zhqj2016@ncist.edu.cn).

**Conflicts of Interest:** The authors declare no conflict of interest.

## References

1. Ghosh, G.; Sivakumar, C. Application of underground microseismic monitoring for ground failure and secure longwall coal mining operation: A case study in an Indian mine. *J. Appl. Geophys.* **2018**, *150*, 21–39. [CrossRef]
2. Zhang, D.; Liu, S.; Guo, D.; Li, Y.; Song, W.; Wang, Y.; Liu, Y. Pipe Piles and Key Stratum Modeling for Grouting Reinforcement of Mine Floors under Mining Disturbance and Microseismic Monitoring Evaluation. *Sustainability* **2023**, *15*, 9294. [CrossRef]
3. Anikiev, D.; Birnie, C.; Waheed, U.B.; Alkhalifah, T.; Gu, C.; Verschuur, D.J.; Eisner, L. Machine learning in microseismic monitoring. *Earth-Sci. Rev.* **2023**, *239*, 104371. [CrossRef]
4. Niu, W.; Feng, X.-T.; Feng, G.; Xiao, Y.; Yao, Z.; Zhang, W.; Hu, L. Selection and characterization of microseismic information about rock mass failure for rockburst warning in a deep tunnel. *Eng. Fail. Anal.* **2021**, *131*, 105910. [CrossRef]
5. Andrés, S.; Santillán, D.; Mosquera, J.C.; Cueto-Felgueroso, L. Thermo-Poroelastic Analysis of Induced Seismicity at the Basel Enhanced Geothermal System. *Sustainability* **2019**, *11*, 6904. [CrossRef]

6. Li, C.C.; Mikula, P.; Simser, B.; Hebblewhite, B.; Joughin, W.; Feng, X.; Xu, N. Discussions on rockburst and dynamic ground support in deep mines. *J. Rock Mech. Geotech. Eng.* **2019**, *11*, 1110–1118. [CrossRef]
7. Chen, B.; Guo, R.; Zeng, K. A nonlinear active noise control algorithm using the FEWT and channel-reduced re-cursive Chebyshev filter. *Mech. Syst. Signal Process.* **2022**, *166*, 108432. [CrossRef]
8. Qu, C.-X.; Yi, T.-H.; Li, H.-N.; Chen, B. Closely spaced modes identification through modified frequency domain decomposition. *Measurement* **2018**, *128*, 388–392. [CrossRef]
9. Qu, C.X.; Yi, T.H.; Li, H.N. Mode identification by eigensystem realization algorithm through virtual frequency response function. *Struct. Control Health Monit.* **2019**, *26*, e2429. [CrossRef]
10. ChunXu, Q.; YuFei, L.; TingHua, Y.; HongNan, L. Structural Damping Ratio Identification through Iterative Frequency Domain Decomposition. *J. Struct. Eng.* **2023**, *149*. [CrossRef]
11. Tang, B.; Jiang, Y.; Zhang, X. Feature extraction method of rolling bearing fault based on singular value decomposition-morphology filter and empirical mode decomposition. *J. Mech. Eng.* **2010**, *46*, 37–48. [CrossRef]
12. Yang, J.; Xu, J.; Yang, D.; Li, M. Noise reduction method for nonlinear time series based on principal manifold learning and its application to fault diagnosis. *Jixie Gongcheng Xuebao (Chin. J. Mech. Eng.)* **2006**, *42*, 154–158. [CrossRef]
13. Zhang, M.; Guo, Y.; Zhang, Z.; He, R.; Wang, D.; Chen, J.; Yin, T. Extraction of pipeline defect feature based on varia-tional mode and optimal singular value decomposition. *Pet. Sci.* **2023**, *20*, 1200–1216. [CrossRef]
14. Yue, Y.; Jiang, T.; Han, C.; Wang, J.; Chao, Y.; Zhou, Q. Suppression of periodic interference during tunnel seis-mic predictions via the Hankel-SVD-ICA method. *J. Appl. Geophys.* **2019**, *168*, 107–117. [CrossRef]
15. Li, Y.; Wang, Y.; Wu, N. Noise suppression method based on multi-scale Dilated Convolution Network in desert seismic data. *Comput. Geosci.* **2021**, *156*, 104910. [CrossRef]
16. Zhang, C.; Shi, Y.; Liu, J.; Jiang, S.; Wang, H.; Wang, Y. A denoising method of mine microseismic signal based on NAEEMD and frequency-constrained SVD. *J. Supercomput.* **2022**, *78*, 17095–17113. [CrossRef]
17. Jackson, G.; Mason, I.; Greenhalgh, S. Principal component transforms of triaxial recordings by singular value decomposition. *Geophysics* **1991**, *56*, 528–533. [CrossRef]
18. Tiwari, R.; Rajesh, R. Factorized Hankel optimal singular spectral approach for erratic and noisy seismic signal denoising. *J. Appl. Geophys.* **2014**, *111*, 95–101. [CrossRef]
19. Lei, B.; Yi, P.; Xiang, J.; Xu, W. A SVD-based signal de-noising method with fitting threshold for EMAT. *IEEE Access* **2021**, *9*, 21123–21131. [CrossRef]
20. Yao, Y.; Liu, L. Automatic P-Wave Arrival Picking based on Inaction Method. *IEEE Trans. Geosci. Remote Sens.* **2022**, *60*, 1–11. [CrossRef]
21. Ma, C.; Yan, W.; Xu, W.; Li, T.; Ran, X.; Wan, J.; Tong, K.; Lin, Y. Parallel Processing Method for Microseismic Signal Based on Deep Neural Network. *Remote Sens.* **2023**, *15*, 1215. [CrossRef]
22. Peng, K.; Guo, H.; Shang, X. EEMD and Multiscale PCA-Based Signal Denoising Method and Its Application to Seismic P-Phase Arrival Picking. *Sensors* **2021**, *21*, 5271. [CrossRef] [PubMed]
23. Chen, H.; Gao, J.; Zhang, B. An adaptive time-varying seismic super-resolution inversion based on $L_p$ regularization. *IEEE Geosci. Remote Sens. Lett.* **2020**, *18*, 1481–1485. [CrossRef]
24. Jiang, J.; Yang, W.; Ren, H. Seismic wavefield information extraction method based on adaptive local singular value decomposition. *J. Appl. Geophys.* **2023**, *210*, 104965. [CrossRef]
25. Ji, G.; Wang, C. A Denoising Method for Seismic Data Based on SVD and Deep Learning. *Appl. Sci.* **2022**, *12*, 12840. [CrossRef]
26. Astuti, W.; Akmeliawati, R.; Sediono, W.; Salami, M. Hybrid technique using singular value decomposition (SVD) and support vector machine (SVM) approach for earthquake prediction. *IEEE J. Sel. Top. Appl. Earth Obs. Remote Sens.* **2014**, *7*, 1719–1728. [CrossRef]
27. Trickett, S. F-xy Cadzow noise suppression. In *SEG Technical Program Expanded Abstracts 2008*; Society of Exploration Geophysicists: Tulsa, OK, USA, 2008; pp. 2586–2590.
28. Oropeza, V.; Sacchi, M. Simultaneous seismic data denoising and reconstruction via multichannel singular spectrum analysis. *Geophysics* **2011**, *76*, V25–V32. [CrossRef]
29. Tian, B.; Ren, H.; Yi, X.; Du, J.; Jiang, C. Noise suppression method for magnetic resonance sounding signals based on double singular value decomposition. *Radio Sci.* **2019**, *54*, 517–530. [CrossRef]
30. Xu, F.; Liu, Y.; Song, J. Feature extraction of acoustic emission signals based on median filter-singular value decomposition and empirical mode decomposition. *Chin. J. Sci. Instrum.* **2011**, *32*, 2712–2716.


**Disclaimer/Publisher's Note:** The statements, opinions and data contained in all publications are solely those of the individual author(s) and contributor(s) and not of MDPI and/or the editor(s). MDPI and/or the editor(s) disclaim responsibility for any injury to people or property resulting from any ideas, methods, instructions or products referred to in the content.